Relative Location Estimation in Wireless Sensor Networks

Neal Patwari, Alfred O. Hero III, Matt Perkins, Neiyer S. Correal and Robert J. O'Dea

Neal Patwari and Alfred O. Hero III are with the University of Michigan, Dept. of EECS, Ann Arbor MI, USA. E-mail: [npatwari, hero]@eecs.umich.edu. Matt Perkins, Neiyer S. Correal, and Robert J. O'Dea are with Motorola Labs, Plantation FL, USA. E-mail: [M.Perkins, N.Correal, Bob.O'Dea]@Motorola.com. This research was partially supported by a NSF Graduate Research Fellowship for the first author, and by ARO-DARPA MURI Grant #DAAD19-02-1-0262

Abstract

Self-configuration in wireless sensor networks is a general class of estimation problems which we study via the Cramér-Rao bound (CRB). Specifically, we consider sensor location estimation when sensors measure received signal strength (RSS) or time-of-arrival (TOA) between themselves and neighboring sensors. A small fraction of sensors in the network have known location while the remaining locations must be estimated. We derive CRBs and maximum-likelihood estimators (MLEs) under Gaussian and log-normal models for the TOA and RSS measurements, respectively. An extensive TOA and RSS measurement campaign in an indoor office area illustrates MLE performance. Finally, relative location estimation algorithms are implemented in a wireless sensor network testbed and deployed in indoor and outdoor environments. The measurements and testbed experiments demonstrate 1 m RMS location errors using TOA, and 1 m to 2 m RMS location errors using RSS.

Index Terms

sensor position location estimation, radio channel measurement, signal strength, time-of-arrival, wireless sensor network testbed, self-configuration, Cramér-Rao bound

I. Introduction

We consider location estimation in networks in which a small proportion of devices, called reference devices, have *a priori* information about their coordinates. All devices, regardless of their absolute coordinate knowledge, estimate the range between themselves and their neighboring devices. Such location estimation is called 'relative location' because the range estimates collected are predominantly between pairs of devices of which neither has absolute coordinate knowledge. These devices without *a priori* information we call blindfolded devices. In cellular location estimation [1][2][3] and local positioning systems (LPS) [4][5], location estimates are made using only ranges between a blindfolded device and reference devices. Relative location estimation requires simultaneous estimation of multiple device coordinates. Greater location estimation accuracy can be achieved as devices are added into the network, even when new devices have no *a priori* coordinate information and range to just a few neighbors.

Emerging applications wireless sensor networks will depend on automatic and accurate location of thousands of sensors. In environmental sensing applications such as water quality monitoring, precision agriculture, and indoor air quality monitoring, "sensing data without knowing the sensor location is meaningless"[6]. In addition, by helping reduce configuration requirements and

device cost, relative location estimation may enable applications such as inventory management [7], intrusion detection [8], traffic monitoring, and locating emergency workers in buildings.

To design a relative location system that meets the needs of these applications, several capabilities are necessary. The system requires a network of devices capable of peer-to-peer range measurement, an ad-hoc networking protocol, and a distributed or centralized location estimation algorithm. For range measurement, using received signal strength (RSS) is attractive from the point of view of device complexity and cost, but is traditionally seen as a coarse measure of range. Time-of-arrival (TOA) range measurement can be implemented using inquiry-response protocols [7][9]. In this article we will show that both RSS and TOA measurements can lead to accurate location estimates in dense sensor networks.

The recent literature has reflected interest in location estimation algorithms for wireless sensor networks [8, 10-16]. Distributed location algorithms offer the promise of solving multi-parameter optimization problems even with constrained resources at each sensor [10]. Devices can begin with local coordinate systems [11] and then successively refine their location estimates [12][13]. Based the shortest path from a device to distant reference devices, ranges can be estimated and then used to triangulate [14]. Distributed algorithms must be carefully implemented to ensure convergence and to avoid 'error accumulation', in which errors propagate serially in the network. Centralized algorithms can be implemented when the application permits deployment of a central processor to perform location estimation. In [15], device locations are resolved by convex optimization. Both [8] and [16] provide maximum likelihood estimators (MLEs) for sensor location estimation, when observations are angle-of-arrival and TOA [8] and when observations are RSS [16].

In this article, we mention only briefly particular location estimation algorithms. Instead, we focus on the accuracy possible using *any* unbiased relative location estimator. The radio channel is notorious for its impairments [17][18], thus sensor location accuracy is limited. The Cramér-Rao bounds (CRBs) presented in this article quantify these limits and allow determination if the accuracies necessary for particular applications are possible.

We begin in Section II by considering CRBs for network self-calibration estimators. Next, we state the relative location estimation problem and derive CRBs and MLEs in Section III. In Section IV, measurements of TOA and RSS are used to illustrate estimator performance. Finally, real-time operation of relative location is demonstrated in Section V. Photos of the experiments

are included in an extended electronic version of this article [19].

II. Network Estimation Bounds

In network self-calibration problems parameters of all devices in a network must be determined. Information comes both from measurements made between pairs of devices and a subset of devices which know *a priori* their parameters. A network self-calibration estimator estimates the unknown device parameters. For example, distributed clock synchronization in a network could be achieved by devices observing pair-wise timing offsets when just a small number of devices are synchronous.

Specifically, consider a vector of device parameters $\boldsymbol{\gamma} = [\gamma_1, \ldots, \gamma_{n+m}]$. Each device has one parameter. Devices $1 \ldots n$ are blindfolded devices and devices $n+1 \ldots n+m$ are reference devices. The unknown parameter vector is $\boldsymbol{\theta} = [\theta_1, \ldots, \theta_n]$ where $\theta_i = \gamma_i$ for $i = 1 \ldots n$. Note $\{\gamma_i, i = n+1 \ldots n+m\}$ are known. Devices i and j make pair-wise observations $X_{i,j}$ with density $f_{X|\boldsymbol{\gamma}}(X_{i,j}|\gamma_i, \gamma_j)$. We allow for the case when devices make incomplete observations, since two devices may be out of range or have limited link capacity. Let $H(i) = \{j : \text{device } j \text{ makes pair-wise observations with device } i\}$. By convention, a device cannot make a pair-wise observation with itself, so that $i \notin H(i)$. By symmetry, if $j \in H(i)$ then $i \in H(j)$.

We assume by reciprocity that $X_{i,j} = X_{j,i}$, thus it is sufficient to consider only the lower triangle of the observation matrix $\mathbf{X} = ((X_{i,j}))_{i,j}$ when formulating the joint likelihood function. In practice, if it is possible to make independent observations on the links from i to j, and from j to i, then we assume that a scalar sufficient statistic can be found. Finally, we assume $\{X_{i,j}\}$ are statistically independent for $j < i$. This assumption can be somewhat oversimplified (see [20] for the RSS case) but necessary for analysis. Using measurements like those in Sections IV and V remains important to verify true performance. The log of the joint conditional pdf is

$$l(\mathbf{X}|\boldsymbol{\gamma}) = \sum_{i=1}^{m+n} \sum_{\substack{j \in H(i) \\ j<i}} l_{i,j}, \quad \text{where } l_{i,j} = \log f_{X|\boldsymbol{\gamma}}(X_{i,j}|\gamma_i, \gamma_j). \tag{1}$$

The CRB on the covariance matrix of any unbiased estimator $\hat{\boldsymbol{\theta}}$ is $\text{cov}(\hat{\boldsymbol{\theta}}) \geq \mathbf{F}_{\boldsymbol{\theta}}^{-1}$, where the Fisher information matrix (FIM) $\mathbf{F}_{\boldsymbol{\theta}}$ is defined as,

$$\mathbf{F}_{\boldsymbol{\theta}} = -\text{E}\nabla_{\boldsymbol{\theta}}(\nabla_{\boldsymbol{\theta}} l(\mathbf{X}|\boldsymbol{\gamma}))^T = \begin{bmatrix} f_{1,1} & \cdots & f_{1,n} \\ \vdots & \ddots & \vdots \\ f_{n,1} & \cdots & f_{n,n} \end{bmatrix} \tag{2}$$

As derived in Appendix A, the diagonal elements $f_{k,k}$ of $\mathbf{F}_{\boldsymbol{\theta}}$ reduce to a single sum over $H(k)$, since there are card$\{H(k)\}$ terms in (1) which depend on $\theta_k = \gamma_k$. The off-diagonal elements can be further reduced: when $k \neq l$, there is at most one summand in (1) which is a function of both k and l.

$$f_{k,l} = \begin{cases} -\sum_{j \in H(k)} \mathrm{E}\left[\frac{\partial^2}{\partial \theta_k^2} l_{k,j}\right], & k = l \\ -\mathrm{I}_{H(k)}(l)\mathrm{E}\left[\frac{\partial^2}{\partial \theta_k \partial \theta_l} l_{k,l}\right], & k \neq l \end{cases} \tag{3}$$

$\mathrm{I}_{H(k)}(l)$ is an indicator function, 1 if $l \in H(k)$ or 0 otherwise.

A. Conditions for a decreasing CRB

Intuitively, as more devices are used for location estimation, the accuracy increases for all of the devices in the network. For an n device network, there are $O(n)$ parameters, but $O(n^2)$ variables $\{X_{i,j}\}$ used for their estimation. The analysis of this section gives sufficient conditions to ensure the CRB decreases as devices are added to the network. Consider a network of n blindfolded devices and m reference devices. Now consider adding one additional blindfolded device. For the n and $(n+1)$ blindfolded device cases, let $\mathbf{F}$ and $\mathbf{G}$ be the FIMs defined in (2), respectively.

Theorem 1: Let $[\mathbf{G}^{-1}]_{ul}$ be the upper left $n \times n$ block of $\mathbf{G}^{-1}$. If for the $(n+1)$ blindfolded device case (1) $\frac{\partial}{\partial \theta_{n+1}} l_{k,n+1} = \pm \frac{\partial}{\partial \theta_k} l_{k,n+1}, \forall k = 1 \ldots n$ and (2) device $n+1$ makes pair-wise observations between itself and at least one blindfolded device and at least two devices, in total; then two properties hold: (1) $\mathbf{F}^{-1} - [\mathbf{G}^{-1}]_{ul} \geq 0$ in the positive semi-definite sense, and (2) $\mathrm{tr}\, \mathbf{F}^{-1} > \mathrm{tr}\, [\mathbf{G}^{-1}]_{ul}$.

Theorem 1 is proven in Appendix B. The Gaussian and log-normal distributions in Section III meet condition (1). Property (1) implies that the additional unknown parameter introduced by the $(n+1)^{st}$ blindfolded device does not impair the estimation of the original n unknown parameters. Furthermore, property (2) implies that the sum of the CRB variance bounds for the n unknown parameters strictly decreases. Thus when a blindfolded device enters a network and makes pair-wise observations with at least one blindfolded device and at least two devices in total, the bound on the average variance of the original n coordinate estimates is reduced. Note that properties (1) and (2) of Theorem 1 would be trivially satisfied by the data processing theorem if adding a device into the network did not increase the number of parameters.

III. Relative Location Estimation

In this section, we specialize for device location estimation using pair-wise RSS or TOA measurements in a wireless network. Specifically, consider a network of m reference and n blindfolded devices. The device parameters $\boldsymbol{\gamma} = [\mathbf{z}_1, \ldots, \mathbf{z}_{m+n}]$ where, for a 2-D system, $\mathbf{z}_i = [x_i, y_i]^T$. The relative location problem corresponds to the estimation of blindfolded device coordinates, $\boldsymbol{\theta} = [\boldsymbol{\theta}_x, \boldsymbol{\theta}_y]$,

$$\boldsymbol{\theta}_x = [x_1, \ldots, x_n], \quad \boldsymbol{\theta}_y = [y_1, \ldots, y_n] \tag{4}$$

given the known reference coordinates $[x_{n+1}, \ldots, x_{n+m}, y_{n+1}, \ldots, y_{n+m}]$. In the TOA case, $X_{i,j} = T_{i,j}$ is the measured TOA between devices i and j in (s), and in the RSS case, $X_{i,j} = P_{i,j}$ is the measured received power at device i transmitted by device j (in mW). As discussed in Section II, only a subset $H(k)$ of devices make pair-wise measurements with device k, $((T_{i,j}))_{i,j}$ and $((P_{i,j}))_{i,j}$ are taken to be upper triangular matrices, and these measurements are assumed statistically independent.

In addition assume that $T_{i,j}$ is Gaussian distributed with mean $d_{i,j}/c$ and variance σ_T^2, denoted:

$$T_{i,j} \sim \mathcal{N}(d_{i,j}/c, \sigma_T^2), \quad d_{i,j} = d(\mathbf{z}_i, \mathbf{z}_j) = \|\mathbf{z}_i - \mathbf{z}_j\|^{1/2} \tag{5}$$

where c is the speed of propagation, and σ_T^2 is not a function of $d_{i,j}$. We assume that $P_{i,j}$ is log-normal, thus the random variable $P_{i,j}(\text{dBm}) = 10 \log_{10} P_{i,j}$ is Gaussian,

$$\begin{aligned} P_{i,j}(\text{dBm}) &\sim \mathcal{N}(\bar{P}_{i,j}(\text{dBm}), \sigma_{dB}^2) \\ \bar{P}_{ij}(\text{dBm}) &= P_0(\text{dBm}) - 10 n_p \log_{10}(d_{i,j}/d_0) \end{aligned} \tag{6}$$

where $\bar{P}_{i,j}(\text{dBm})$ is the mean power in dBm, σ_{dB}^2 is the variance of the shadowing, and $P_0(\text{dBm})$ is the received power at a reference distance d_0. Typically $d_0 = 1$ meter, and P_0 is calculated from the free space path loss formula [21]. The path loss exponent n_p is a function of the environment. For particular environments, n_p may be known from prior measurements. Although we derive the CRB assuming n_p is known, it could have been handled as an unknown 'nuisance' parameter.

Given (6), the density of $P_{i,j}$ is,

$$\begin{aligned} f_{P|\boldsymbol{\gamma}}(P_{i,j}|\boldsymbol{\gamma}) &= \tfrac{10/\log 10}{\sqrt{2\pi\sigma_{dB}^2}} \tfrac{1}{P_{i,j}} \exp\left[-\tfrac{b}{8} \left(\log \tfrac{d_{i,j}^2}{\tilde{d}_{i,j}^2} \right)^2 \right] \\ \text{where} \quad b &= \left(\tfrac{10 n_p}{\sigma_{dB} \log 10} \right)^2, \quad \tilde{d}_{i,j} = d_0 \left(\tfrac{P_0}{P_{i,j}} \right)^{\frac{1}{n_p}}. \end{aligned} \tag{7}$$

Here $\tilde{d}_{i,j}$ is the MLE of range $d_{i,j}$ given received power $P_{i,j}$.

Neither $P_{i,j}$ nor $T_{i,j}$ are assumed to be ergodic random variables – in fact, obstructions in the measured environment that cause shadowing and TOA errors do not usually change over time. The CRB gives a lower bound on the ensemble variance over different random shadowing environments. If networks with the same relative device coordinates are implemented in many different areas, the variances of any unbiased coordinate estimator will be lower bounded by the CRB presented here.

The model assumptions made in this section will justified by experiment in Section IV. In the next sections, we use these models to derive the CRB and MLE for both RSS and TOA measurements.

A. One-Dimensional TOA Example

Consider using TOA measurements to locate devices that are limited to a one-dimensional linear track. This could, for example, be applied to location estimation on an assembly line. Consider n blindfolded devices and m reference devices with combined parameter vector $\boldsymbol{\gamma} = [x_1, \ldots, x_{n+m}]$. The unknown coordinate vector is $\boldsymbol{\theta} = [x_1, \ldots, x_n]$. Assume all devices make pair-wise measurements with every other device, ie., $H(k) = \{1, \ldots, k-1, k+1, \ldots, m+n\}$. The distribution of the observations is given by (5) with $d_{i,j} = |x_j - x_i|$. The second partials of $l_{i,j}$ are, $\frac{\partial^2}{\partial x_j^2} l_{i,j} = -\frac{\partial^2}{\partial x_j \partial x_i} l_{i,j} = \frac{-1}{\sigma_T^2 c^2}$, $\forall i \neq j$, which are constant with respect to the random variables $T_{i,j}$. Thus the FIM, calculated using (3), is $\mathbf{F}_T = [(n+m)\mathbf{I}_n - \underline{1}\underline{1}^T]/(\sigma_T c)^2$, where $\mathbf{I}_n$ is the $n \times n$ identity matrix, and $\underline{1}$ is a n by 1 vector of ones. For $m \geq 1$, the matrix is invertible,

$$\mathbf{F}_T^{-1} = \frac{\sigma_T^2 c^2}{m(n+m)} \left[m\mathbf{I}_n + \underline{1}\underline{1}^T \right].$$

The CRB on the variance of an unbiased estimator for x_i is,

$$\sigma_{x_i}^2 \geq \sigma_T^2 c^2 \frac{m+1}{m(n+m)}. \tag{8}$$

Expression (8) implies that the variance $\sigma_{x_i}^2$ is reduced more quickly by adding reference (m) than blindfolded (n) devices. However, if m is large, the difference between increasing m and n is negligible.

B. Two-Dimensional Location Estimation

In the remainder of this article, we focus on 2-D location estimation of (4). We denote by $\mathbf{F}_R$ and $\mathbf{F}_T$ the FIMs for the RSS and TOA measurements, respectively. Each device has two

parameters, and we can see that the FIM will have a similar form to (2) if partitioned into blocks,

$$\mathbf{F}_R = \begin{bmatrix} \mathbf{F}_{Rxx} & \mathbf{F}_{Rxy} \\ \mathbf{F}_{Rxy}^T & \mathbf{F}_{Ryy} \end{bmatrix}, \quad \mathbf{F}_T = \begin{bmatrix} \mathbf{F}_{Txx} & \mathbf{F}_{Txy} \\ \mathbf{F}_{Txy}^T & \mathbf{F}_{Tyy} \end{bmatrix} \tag{9}$$

where $\mathbf{F}_{Rxx}$ and $\mathbf{F}_{Txx}$ are given by (2) using only the x parameter vector $\boldsymbol{\theta} = \boldsymbol{\theta}_x$, and $\mathbf{F}_{Ryy}$ and $\mathbf{F}_{Tyy}$ are given by (2) using only $\boldsymbol{\theta} = \boldsymbol{\theta}_y$. The off-diagonal blocks $\mathbf{F}_{Rxy}$ and $\mathbf{F}_{Txy}$ are similarly derived. The elements of the sub-matrices of (9) are derived in Appendix C. For the case of RSS measurements, the elements are given by,

$$\begin{aligned}
\left[\mathbf{F}_{Rxx}\right]_{k,l} &= \begin{cases} b\sum_{i\in H(k)} \frac{(x_k-x_i)^2}{[(x_k-x_i)^2+(y_k-y_i)^2]^2} & k=l \\ -b\,\mathrm{I}_{H(k)}(l)\frac{(x_k-x_l)^2}{[(x_k-x_l)^2+(y_k-y_l)^2]^2} & k\neq l \end{cases} \\
\left[\mathbf{F}_{Rxy}\right]_{k,l} &= \begin{cases} b\sum_{i\in H(k)} \frac{(x_k-x_i)(y_k-y_i)}{[(x_k-x_i)^2+(y_k-y_i)^2]^2} & k=l \\ -b\,\mathrm{I}_{H(k)}(l)\frac{(x_k-x_l)(y_k-y_l)}{[(x_k-x_l)^2+(y_k-y_l)^2]^2} & k\neq l \end{cases} \\
\left[\mathbf{F}_{Ryy}\right]_{k,l} &= \begin{cases} b\sum_{i\in H(k)} \frac{(y_k-y_i)^2}{[(x_k-x_i)^2+(y_k-y_i)^2]^2} & k=l \\ -b\,\mathrm{I}_{H(k)}(l)\frac{(y_k-y_l)^2}{[(x_k-x_l)^2+(y_k-y_l)^2]^2} & k\neq l \end{cases}
\end{aligned} \tag{10}$$

For the case of TOA measurements, the elements are,

$$\begin{aligned}
\left[\mathbf{F}_{Txx}\right]_{k,l} &= \begin{cases} \frac{1}{c^2\sigma_T^2}\sum_{i\in H(k)} \frac{(x_k-x_i)^2}{(x_k-x_i)^2+(y_k-y_i)^2} & k=l \\ -\frac{1}{c^2\sigma_T^2}\mathrm{I}_{H(k)}(l)\frac{(x_k-x_l)^2}{(x_k-x_l)^2+(y_k-y_l)^2} & k\neq l \end{cases} \\
\left[\mathbf{F}_{Txy}\right]_{k,l} &= \begin{cases} \frac{1}{c^2\sigma_T^2}\sum_{i\in H(k)} \frac{(x_k-x_i)(y_k-y_i)}{(x_k-x_i)^2+(y_k-y_i)^2} & k=l \\ -\frac{1}{c^2\sigma_T^2}\mathrm{I}_{H(k)}(l)\frac{(x_k-x_l)(y_k-y_l)}{(x_k-x_l)^2+(y_k-y_l)^2} & k\neq l \end{cases} \\
\left[\mathbf{F}_{Tyy}\right]_{k,l} &= \begin{cases} \frac{1}{c^2\sigma_T^2}\sum_{i\in H(k)} \frac{(y_k-y_i)^2}{(x_k-x_i)^2+(y_k-y_i)^2} & k=l \\ -\frac{1}{c^2\sigma_T^2}\mathrm{I}_{H(k)}(l)\frac{(y_k-y_l)^2}{(x_k-x_l)^2+(y_k-y_l)^2} & k\neq l \end{cases}
\end{aligned} \tag{11}$$

Note $\mathbf{F}_R \propto n_p^2/\sigma_{dB}^2$ while $\mathbf{F}_T \propto 1/(c^2\sigma_T^2)$. These SNR quantities directly affect the CRB. For TOA measurements, the dependence on the device coordinates is in unit-less distance ratios, indicating that the size of the system can be scaled without changing the CRB as long as the geometry is kept the same. However, in the case of RSS measurements, the variance bound scales with the size of the system even if the geometry is kept the same due to the d^4 terms in the denominator of each term of $\mathbf{F}_R$. These scaling characteristics indicate that TOA measurements would be preferred for sparse networks, but for sufficiently high density, RSS can perform as well as TOA.

Let $\hat{x}_i$ and $\hat{y}_i$ be unbiased estimators of x_i and y_i. For the case of TOA measurements, the

trace of the covariance of the i^{th} location estimate satisfies

$$\begin{aligned}\sigma_i^2 &\triangleq \operatorname{tr}\left\{\operatorname{cov}_{\boldsymbol{\theta}}(\hat{x}_i,\hat{y}_i)\right\} = \operatorname{Var}_{\boldsymbol{\theta}}(\hat{x}_i) + \operatorname{Var}_{\boldsymbol{\theta}}(\hat{y}_i) \\ &\geq \left(\left[\mathbf{F}_{Txx} - \mathbf{F}_{Txy}\mathbf{F}_{Tyy}^{-1}\mathbf{F}_{Txy}^T\right]^{-1}\right)_{i,i} + \\ &\quad \left(\left[\mathbf{F}_{Tyy} - \mathbf{F}_{Txy}\mathbf{F}_{Txx}^{-1}\mathbf{F}_{Txy}^T\right]^{-1}\right)_{i,i} \end{aligned} \tag{12}$$

For RSS measurements, replace $\mathbf{F}_T$ in (12) with $\mathbf{F}_R$. For the case of one blindfolded device, a simple expression can be derived for both RSS and TOA measurements.

C. Single Unknown Location Example

Consider the network having blindfolded device 1 and reference devices $2 \ldots m+1$. This example, with a single pair of unknowns x_1 and y_1, is equivalent to many existing location systems, and a bound for the variance of the location estimator has already been derived in for TOA measurements [2]. In the case of RSS measurements,

$$\sigma_1^2 \triangleq E\left[(\hat{x}_1 - x_1)^2 + (\hat{y}_1 - y_1)^2\right] \geq \frac{F_{Rxx} + F_{Ryy}}{F_{Rxx}F_{Ryy} - F_{Rxy}^2},$$

from which we obtain

$$\sigma_1^2 = \frac{1}{b}\frac{\sum_{i=2}^{m+1} d_{1,i}^{-2}}{\sum_{i=2}^{m}\sum_{j=i+1}^{m+1}\left(\frac{d_{1\perp i,j}d_{i,j}}{d_{1,i}^2 d_{1,j}^2}\right)^2},$$

where the distance $d_{1\perp i,j}$ is the shortest distance from the point (x_1, y_1) to the line segment connecting device i and device j. For the case of TOA measurements, we obtain

$$\sigma_1^2 = c^2\sigma_T^2 m\left[\sum_{i=2}^{m}\sum_{j=i+1}^{m+1}\left(\frac{d_{1\perp i,j}d_{i,j}}{d_{1,i}d_{1,j}}\right)^2\right]^{-1} \tag{13}$$

The ratio $d_{1\perp i,j}d_{i,j}/(d_{1,i}d_{1,j})$ has been called the geometric conditioning $\mathcal{A}_{i,j}$ of device 1 w.r.t. references i and j [2]. $\mathcal{A}_{i,j}$ is the area of the parallelogram specified by the vectors from device 1 to i and from device 1 to j, normalized by the lengths of the two vectors. The geometric dilution of precision (GDOP), defined as $\sigma_1/(c\sigma_T)$, is

$$GDOP = \sqrt{\frac{m}{\sum_{i=1-m}^{-1}\sum_{j=i+1}^{0}\mathcal{A}_{i,j}^2}}$$

which matches the result in [2]. The CRBs are shown in Fig. 1 when there are four reference devices located in the corners of a 1m by 1m square. The minimum of Fig. 1(a) is 0.27. Since

the CRB scales with size in the RSS case, the standard deviation of unbiased location estimates in a traditional RSS system operating in a channel with $\sigma_{dB}/n_p = 1.7$ is limited to about 27% of the distance between reference devices. This performance has prevented use of RSS in many existing location systems and motivates having many blindfolded devices in the network. Note in the TOA case, σ_1 is proportional to $c\sigma_T$, thus $c\sigma_T = 1$ was chosen in Fig. 1(b).

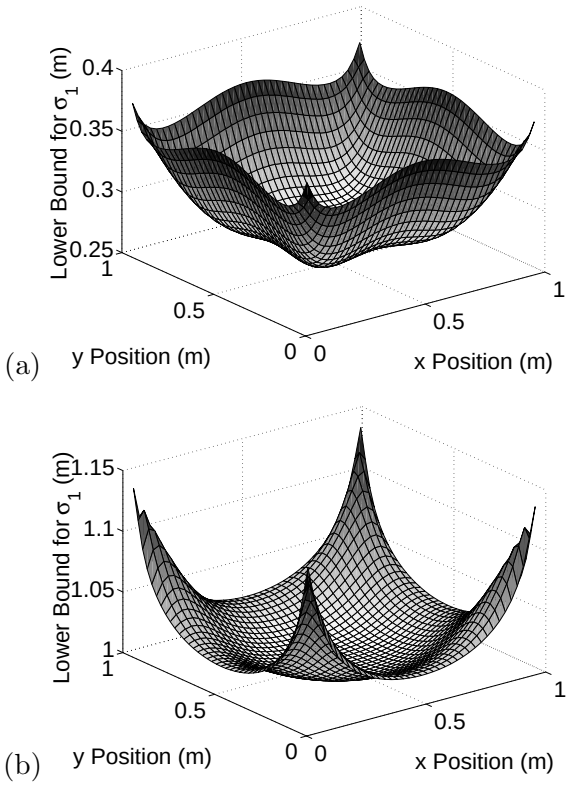

Fig. 1. σ_1 (m) for the example system vs. the coordinates of the single blindfolded device, for (a) RSS with $\sigma_{dB}/n = 1.7$, or (b) TOA with $c\,\sigma_T = 1$m.

D. Maximum Likelihood Relative Location Estimation

For general n and m, we calculate the MLE of $\boldsymbol{\theta}$. In the case of TOA measurements, the MLE is

$$\hat{\boldsymbol{\theta}}_T = \arg\min_{\{\mathbf{z}_i\}} \sum_{i=1}^{m+n} \sum_{\substack{j \in H(i) \\ j<i}} \left(c\,T_{i,j} - d(\mathbf{z}_i, \mathbf{z}_j)\right)^2, \tag{14}$$

where $\mathbf{z}_i = [x_i, y_i]^T$. The MLE for the RSS case is [16],

$$\hat{\boldsymbol{\theta}}_{\tilde{R}} = \arg\min_{\{\mathbf{z}_i\}} \sum_{i=1}^{m+n} \sum_{\substack{j \in H(i) \\ j<i}} \left(\ln \frac{\tilde{d}_{i,j}^2}{d^2(\mathbf{z}_i, \mathbf{z}_j)}\right)^2 \tag{15}$$

Unlike the MLE based on TOA measurements, the RSS MLE is readily shown to be biased. Specifically, for a single reference and single blindfolded device, the range estimate between the two devices is $\tilde{d}_{1,2}$. Using (7), the mean of $\tilde{d}_{1,2}$ is given by

$$E[\tilde{d}_{1,2}] = C\, d_{1,2}, \quad \text{where } C = \exp\left[\frac{1}{2}\left(\frac{ln(10)}{10}\frac{\sigma_{dB}}{n_p}\right)^2\right] \tag{16}$$

For typical channels [21], $C \approx 1.2$, adding 20% bias to the range. Motivated by (16), a bias-reduced MLE can be defined,

$$\hat{\boldsymbol{\theta}}_R = \arg\min_{\{\mathbf{z}_i\}} \sum_{i=1}^{m+n} \sum_{\substack{j\in H(i)\\ j<i}} \left(\ln \frac{\tilde{d}_{i,j}^2/C^2}{d^2(\mathbf{z}_i, \mathbf{z}_j)}\right)^2 \tag{17}$$

However, there remains residual bias. Consider $m = 4$ and $n = 1$. Place the reference devices at the corners of a 1 m by 1 m square and the blindfolded device within the square, the same as the case plotted in Fig. 1. We calculate via simulation [22] the bias gradient norm of $\hat{x}_1$ given by (17) and display it in Fig. 2.

The gradient of the bias can be used in the uniform CRB to calculate the achievable variance of the biased estimator [22] as compared to all other estimators with same or less bias gradient norm. Fig. 2 shows that the bias gradient is high (with norm ≈ 1) at the corners of the square. Expression (17) shows that the MLE tries to force the ratio $\tilde{d}_{1,j}^2/(C^2 d_{1,j}^2)$ close to 1. If the blindfolded device is very close to one reference device and far away from the others, then measurements from the other three reference devices provide relatively little information regarding the placement of the blindfolded device. In the limit as the blindfolded device approaches a reference device, it can only be localized to a circle around that reference. Thus no unbiased estimator is possible. The MLE in (17) approaches a constant in the limit, and thus the bias gradient norm approaches 1.

IV. Channel Measurement Experiment

In this section, we describe the measurement system and experiment and validate the channel model assumptions made at the beginning of Section III. A set of multipoint-to-multipoint (M2M) wideband channel measurements were conducted at the Motorola facility in Plantation, Florida. The measurement environment is an office area partitioned by 1.8m high cubicle walls, with hard partitioned offices, external glass windows and cement walls on the outside of the area. There are also metal and concrete support beams within and outside of the area. Offices are

occupied with desks, bookcases, metal and wooden filing cabinets, computers and equipment. Forty-four device locations are identified within a 14m by 13m area and marked with tape.

The measurement system uses a wideband direct-sequence spread-spectrum (DS-SS) transmitter (TX) and receiver (RX) (Sigtek model ST-515). The TX and RX are battery-powered and are placed on carts. The TX outputs an unmodulated pseudo-noise (PN) code signal with a 40 MHz chip rate and code length 1024. The center frequency is 2443 MHz, and the transmit power is 10 mW. Both TX and RX use 2.4 GHz sleeve dipole antennas kept 1m above the floor. The antennas have an omnidirectional pattern in the horizontal plane and a measured antenna gain of 1.1 dBi. The RX records I and Q samples at a rate of 120 MHz, downconverts, and correlates them with the known PN signal and outputs a power-delay profile (PDP). An example PDP is shown in Fig. 4. We ensure that noise and ISM-band interference is not an issue by maintaining an SNR > 25 dB throughout the campaign.

For TOA, wireless sensors will likely make two-way (round-trip) measurements [7][9] due to the impracticality of accurately synchronizing all devices in wireless sensor networks. Two-way TOA measurements do not require synchronized devices since the round-trip delay can be measured at a single device and then divided by two to estimate the one-way propagation time. However, for the purpose of these measurements, two-way TOA measurements are not necessary. Instead, we carefully synchronize our TX and RX using off-the-shelf time-synchronization equipment. Errors due to multipath are the predominant source of variance in TOA estimates: for the two-way TOA case this has been reported in [9], and for these measurements this is demonstrated below. One-way synchronized and two-way TOA measurements are equally affected by the multipath channel, thus this one-way measurement experiment closely approximates the TOAs that would

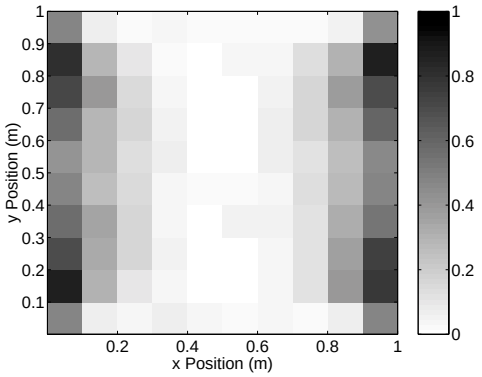

Fig. 2. Bias gradient norm of the RSS MLE of x_1 from (17) for the example system of Section III-C.

Fig. 3. Photo of measurement area looking above cubicle walls.

be measured in a sensor network.

Both TX and RX are synchronized by 1 pulse per second (1PPS) signals from two Datum ExacTime GPS and rubidium-based oscillators. On each of the eight days of the campaign, a procedure is followed to ensure a stable time base. After an initial GPS synch of the ExacTimes, GPS is disconnected and the rubidium oscillators provide stable 1PPS signals. The frequencies of the two rubidium oscillators are off very slightly, thus the 1PPS signals drift linearly, on the order of ns per hour. By periodically measuring and recording the offset between the two 1PPS signals using an oscilloscope, the effect of the linear drift can be cancelled. A time base with a standard deviation of between 1-2 ns is achieved. The variance of the time base ($\leq 4\text{ns}^2$) is thus a small source of error in the measured TOA variance (37ns^2) reported in Section IV-A.

The M2M measurements are conducted by first placing the TX at location 1 while the RX is moved and measurements are made at locations 2 through 44. Then the TX is placed at location 2, as the RX is moved to locations 1 and 3 through 44. At each combination of TX and RX locations, the RX records five PDPs. Since we expect reciprocity, there are a total of 10 measurements for each link. All devices are in range of all other devices. Over the course of the 8-day campaign, a total of 44*43*5 = 9460 measurements are taken.

A. Estimating TOA and RSS

The wideband radio channel impulse response (CIR) is modeled as a sum of attenuated, phase-shifted, and time-delayed multipath impulses [18][21]. The PDP output of the Sigtek measurement system, due to its finite bandwidth, replaces each impulse of the CIR with the autocorrelation function of the PN signal $R_{PN}(\tau)$ shown in Fig. 4(c), an approximately triangular

peak $2/R_C = 50$ns wide. In high SNR, low multipath cases, TOA estimates can be more accurate than $2/R_C$. However, a wider peak permits more multipath errors since the line-of-sight (LOS) component, with TOA $d_{i,j}/c$, can be obscured by non-LOS multipath that arrive $< 2/R_C$ seconds after the LOS TOA. If the LOS component is attenuated, it can be difficult to distinguish the LOS TOA. In Fig. 4(a), the PDP is seen to contain several multipath within the first 200ns. Inspecting the PDP immediately after $\tau = 0$, as shown in Fig. 4(b), the LOS path at 42ns is visible but attenuated compared to a later multipath which appears to arrive at 80ns.

The template-matching method [23] provides a TOA estimation algorithm which is robust to such attenuated-LOS multipath channels. In template-matching, samples of the leading edge of the PDP are compared to a normalized and oversampled template of $R_{PN}(\tau)$ shown in Fig. 4(c). The TOA estimate $\tilde{t}_{i,j}$ is the delay that minimizes the squared-error between the samples of the PDP and the template. In Fig. 4(b), the template-matching TOA estimate $\tilde{t}_{1,24} = 51$ns is in error by +9ns. If a local maxima was necessary to identify the LOS path, the error would have been much greater.

Since non-LOS multipath are delayed in time, $\tilde{t}_{i,j}$ usually has a positive bias. We estimate the bias to be the average of $\tilde{t}_{i,j} - d_{i,j}/c$, $\forall i, j$ which in these measurements is 10.9 ns. In this paper we assume this bias is known for environments of interest, however, and, similarly to n_p, this bias could be estimated as a 'nuisance' parameter. Subtracting out the bias from our measurements, we get the unbiased TOA estimator $t_{i,j}$. Finally, the average of the 10 $t_{i,j}$ measurements for the

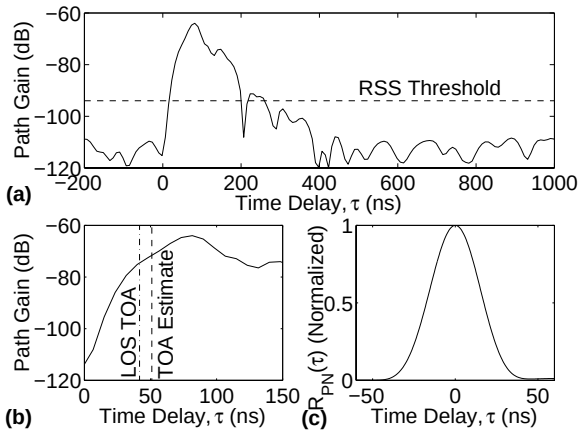

Fig. 4. (a) Measured PDP with TX at 1 and RX at 24 and threshold (- - -) above which received power is integrated to calculate RSS. (b) Leading edge of same PDP showing LOS TOA $= d_{1,24}/c$ ($\cdot - \cdot - \cdot$) and estimated TOA (- - -). (c) Autocorrelation of PN signal $R_{PN}(\tau)$ used in template-matching [23].

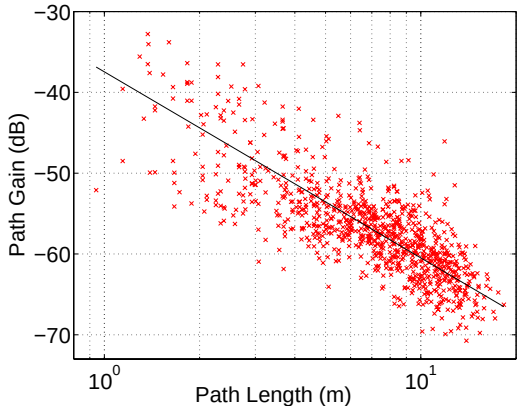

Fig. 5. Measured wideband path gain (x) as a function of path length. Linear fit (—) is with $d_0 = 1$m, $n_p = 2.3$, and $\sigma_{dB} = 3.92$.

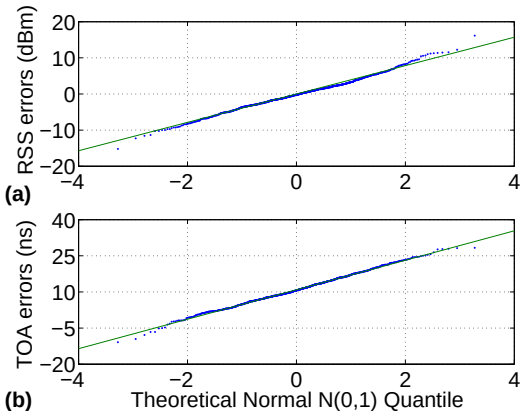

Fig. 6. Q-Q plot of (a) $P_{i,j}(\text{dBm}) - \bar{P}_{i,j}(\text{dBm})$ for RSS data, and (b) $T_{i,j} - d_{i,j}/c$ for TOA data, compared to a Gaussian quantile.

link between i and j we call $T_{i,j}$. The measured standard deviation, σ_T, is 6.1 ns.

It has been shown that a wideband estimate of received power, $p_{i,j}$, can be obtained by summing the powers of the multipath in the PDP [21]. To distinguish between noise and multipath, only power above a noise threshold is summed, as shown in Fig. 4(a). This wideband method reduces the frequency-selective fading effects. The geometric mean of the 10 $p_{i,j}$ measurements for the link between i and j, which we call $P_{i,j}$, reduces fading due to motion of objects in the channel. Shadowing effects, caused by permanent obstructions in the channel, remain predominant in $P_{i,j}$ since the TX and RX are stationary. Shadowing loss is often reported to be a log-normal random variable [18][21][24], which lead us to propose the log-normal shadowing model in (6). As shown in Fig. 5, The measured $P_{i,j}$ match the log-normal shadowing model in

(6) with $n = 2.30$ and $\sigma_{dB} = 3.92$ dB, using $d_0 = 1$m. The low variance may be due to the wide bandwidth, averaging, and homogeneity of the measured cubicle area.

We verify the log-normal and Gaussian distributions of the RSS and TOA measurements by examining the residuals $r_{i,j}^R \triangleq P_{i,j}(\text{dBm}) - \bar{P}_{i,j}(\text{dBm})$ and $r_{i,j}^T \triangleq T_{i,j} - d_{i,j}/c$ via quantile-quantile plots in Fig. 6. Both RSS and TOA data fit the models well between the -2 and +2 quantiles. Using a Kolmogorov-Smirnov (KS) test, we test the hypothesis: $H_0 : r_{i,j}^R \sim \mathcal{N}(\bar{r}^R, S_R^2)$ vs. $H_1 : r_{i,j}^R$ is not Gaussian, where $\bar{r}^R$ is the sample mean of $r_{i,j}^R$ and S_R^2 is the sample variance. An identical test is conducted on $r_{i,j}^T$ for the TOA measurements. For the RSS and TOA residuals, the KS tests yield p-values of 0.09 and 0.50, respectively. In both cases, we would decide to accept H_0 at a level of significance of $\alpha = 0.05$.

However, the low p-value for the RSS data indicates that log-normal shadowing model in (6) may not fully characterize the data. In fact, if we use in H_0 a 2-component Gaussian mixture distribution (with parameters estimated from $r_{i,j}^R$ via the MLE), the KS test yields a p-value of 0.88. A topic for future research is to investigate whether the potential benefits of using a mixture distribution in the channel model would justify its additional complexity. The experimental results reported in the next sections use only the MLE derived under the log-normal shadowing model; these results nevertheless demonstrate good location accuracy.

B. Location Estimates from Measurements

Four devices near the corners are chosen as reference devices. The remaining 40 devices are blindfolded devices. The four reference device coordinates and either the RSS or TOA measurements, $P_{i,j}$ or $T_{i,j}$, are input to the MLE in (17) or (14). The minimum in each case is found via a conjugate gradient algorithm. Then,the estimated device locations are compared to the actual locations in Fig. 7(a) and (b). To generalize the results, the RMS location error of all 40 unknown-location devices is 2.18m in the RSS case and 1.23m in the TOA case. Since shadowing and non-LOS errors are not ergodic, as discussed in Section IV-A, experimentally determining the MLE variances would require several measurement campaigns with the same device geometry but in different office areas. This was not possible due to resource and time limitations. Nevertheless, it is instructive to report the CRB for the measured network. We use the measured channel parameters, $\sigma_{dB}/n_p = 1.70$ and $\sigma_T = 6.1$ ns, the four reference devices used above, and the actual coordinates of all of the devices to calculate the CRB for σ_i^2 given in

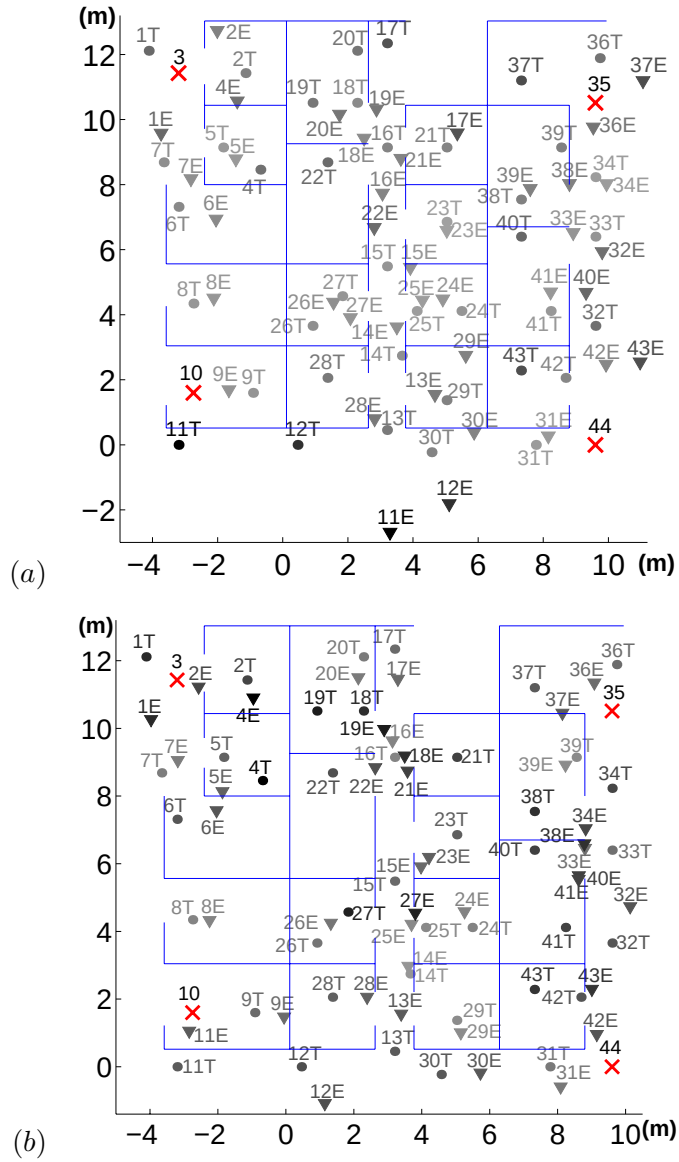

Fig. 7. True (•#T) and estimated (▼#E) location using (a) RSS and (b) TOA data for measured network with 4 reference devices (X#). Higher errors are indicated by darker text.

(12) for $i = 1 \ldots n$ and for both TOA and RSS measurements. The quantity $\left(\sum_{i=1}^{40} \sigma_i^2/40\right)^{1/2}$ is lower bounded by 0.76m for the RSS and 0.69m for the TOA cases.

We also notice that the devices close to the center are located more accurately than the devices on the edges, particularly in the RSS case. Poor performance at the edges is expected since devices have fewer nearby neighbors to benefit their location estimate.

V. Testbed Experimentation

To provide an easy means for M2M radio channel measurement and location estimation testing, we developed and fabricated at Motorola Labs a testbed of 12 prototype peer-to-peer wireless sensor devices with RSS measurement capability. The devices have FSK transceivers with a 50 kHz data rate which operate in the 900-928 MHz band at one of 8 center frequencies separated by 4 MHz, which is approximately the coherence bandwidth of the channel. Devices hop between center frequencies so that RSS measurements can be taken at each center frequency. While one device transmits, other devices measure its RSS. Packet transmissions are infrequent and packets are short, thus the channel is almost always silent. Devices are asynchronous and use a carrier-sense multiple access (CSMA) protocol. Thus RX measurements are not subject to multi-user interference. Every two seconds, each device creates a packet of measured RSS data and transmits it to a central 'listening' device, which uploads data to a laptop computer. The laptop has access to the known coordinates of the reference devices and the TX power and the RSS characteristic of the devices as measured prior to deployment. The laptop stores the RSS for each pair of devices, each frequency, and each measurement over time.

First, we use the testbed as an easy way to estimate the path loss exponent n_p. When all of the device locations are known, the laptop uses the path loss vs. path length data to estimate the path loss exponent, n_p [25]. After estimating n_p, the blindfolded device coordinates are removed from the laptop and we operate the relative location estimation algorithm using the estimated n_p.

Next, the relative location estimation algorithm averages the measurements over time (using the most recent four RSS measurements), frequency (across 8 center frequencies), and the reciprocal channel, resulting in the averaged measurement $P_{i,j}$. The maximum of the MLE in (17) is found using a conjugate gradient algorithm, which takes less than one second on the Pentium laptop. Each second an updated location is calculated and displayed on a map in a Visual Basic GUI. Real time tracking of slow movement (eg., people walking) is possible.

A. Parking Lot Area

Testbed devices are placed in a 9 m by 9 m area in a 3 m grid in an empty parking lot area at the Motorola facility. Devices are kept at a height of 0.35 m. Using the testbed, we estimate n_p to be 3.2. Then, we place reference devices at the four corners of the area and blindfolded

Fig. 8. Parking lot testbed experiment, showing grid of devices, located on top of upside-down recycling bins.

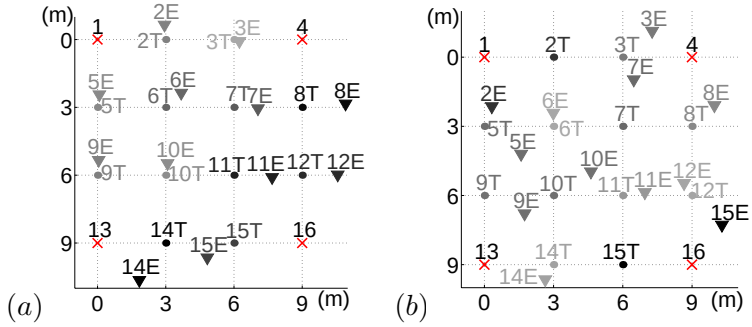

Fig. 9. True (•#T) and estimated (▼#E) location for the (a) parking lot and (b) residential home tests, using 4 reference devices (X#). Higher errors are indicated by darker text.

devices at 7 of the remaining 12 spots in the grid (for 11 devices total). Devices record RSS and send packets as described above. The blindfolded devices are then moved to different positions in the grid for a new trial. 16 trials are run. The RMS location errors for the individual trials range from 0.9 m to 2.4 m. However, by moving 7 blindfolded devices around between positions, we record enough point-to-point ranges to see what would happen if there were 12 blindfolded devices, one in each spot on the grid. We use the recorded range data off-line to calculate that the RMS error would have been 1.46 m. Furthermore, if we extended the duration of the time averaging from 4 to 32 ranges, we would see the location estimates shown in Fig. 9(a), and the RMS error would reduce to 1.02 m. Since shadow fading is not severe in this environment, time averaging is effective at improving location estimates.

B. Residential Home

Next, we test the system in the Perkins home, a single-family, ranch-style house in Sunrise, Florida (Fig. 10). An identical 9 m by 9 m grid is used in this test, which spanned across many interior rooms and an outdoor patio. The obstructions include indoor walls, furnishings,

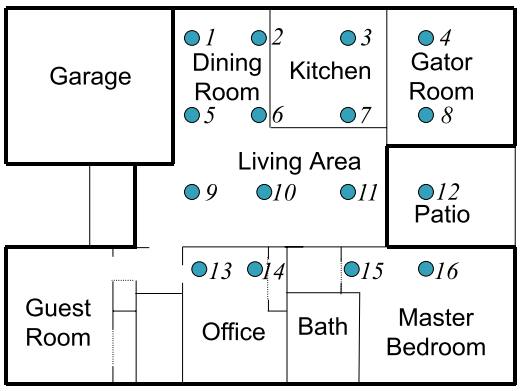

Fig. 10. Map of the grid of sensors in the Perkins home.

Fig. 11. Residential home testbed experiment, with 3 devices shown (one is hidden between the couch and the table).

appliances, and exterior walls & windows, and n_p is estimated to be 4.0. Here, there are 4 reference devices in the corners of the grid and 8 other blindfolded devices. In 16 individual trials, the RMS location errors range from 1.0 m to 2.7 m. If all device ranges are used together, as described previously, we see the results in Fig. 9(b), in which the RMS error is 2.1 m. This error doesn't reduce significantly when the duration of time-averaging is increased from 4 to 32 ranges. Much of the error is due to device #15, which has an error of 4.5 m. As seen in Fig. 10, $d_{14,15} = 3$ m, but significant shadowing is caused by the office closet and master bedroom closet that both lie directly in between the two devices ($P_{14,15}(\text{dBm}) - \bar{P}_{14,15}(\text{dBm}) = -22$), and as

a result the range estimate between the two is 10.5 m. Unfortunately, this shadowing can't be countered by time or frequency averaging.

VI. Conclusions

The motivation of this article has been to show the accuracy with which wireless sensor networks can estimate the relative sensor locations. The results should help researchers determine if the accuracy possible from relative location estimation can meet their application requirements. This article began by proving that location estimation variance bounds (CRB) decrease as more devices are added to the network. Next, it was shown that CRBs can be readily calculated for arbitrary numbers and geometries of devices, and several examples were presented. Sensor location estimation with approximately 1 m RMS error has been demonstrated using TOA measurements. However, despite the reputation of RSS as a coarse means to estimate range, it can nevertheless achieve an accuracy of about 1 m RMS in a testbed experiment. Fading outliers can still impair the RSS relative location system, implying the need for a robust estimator. Future experimentation is needed to verify the variance of location estimators due to the non-ergodic nature of shadowing. Analysis can quantify the effect of 'nuisance' channel parameters, and can be extended to consider the effects of multi-user interference on sensor location estimation.

Appendix

A. CRB for Network Self-Calibration

The diagonal elements, $f_{k,k}$, of $\mathbf{F}$ given in (2) are,

$$\begin{aligned} f_{k,k} &= \mathrm{E}\left(\tfrac{\partial}{\partial\theta_k} l(\mathbf{X}|\boldsymbol{\theta})\right)^2 = \mathrm{E}\Big(\sum_{j\in H(k)} \tfrac{\partial}{\partial\theta_k} l_{k,j}\Big)^2 \\ f_{k,k} &= \sum_{j\in H(k)} \sum_{p\in H(k)} \mathrm{E}\left(\tfrac{\partial}{\partial\theta_k} l_{k,j}\right)\left(\tfrac{\partial}{\partial\theta_k} l_{k,p}\right) \end{aligned}$$

Since $X_{k,j}$ and $X_{k,p}$ are independent random variables, and $E[\frac{\partial}{\partial\theta_k} l_{k,j}] = 0$, the expectation of the product is only nonzero for $p = j$. Thus $f_{k,k}$ simplifies to the $k = l$ result in (3). The off-diagonal elements similarly simplify,

$$f_{k,l} = \sum_{j\in H(k)} \sum_{p\in H(l)} \mathrm{E}\left(\tfrac{\partial}{\partial\theta_k} l_{k,j}\right)\left(\tfrac{\partial}{\partial\theta_l} l_{l,p}\right)$$

Here, due to independence and zero mean of the two terms, the expectation of the product will be zero unless both $p = k$ and $j = l$. Thus the $k \neq l$ result in (3).

B. Proof of Theorem 1

Compare $\mathbf{F}$, the FIM for the n blindfolded device problem, to $\mathbf{G}$, the FIM for the $n+1$ blindfolded device case. Partition $\mathbf{G}$ into blocks,

$$\mathbf{G} = \begin{bmatrix} \mathbf{G}_{ul} & \mathbf{g}_{ur} \\ \mathbf{g}_{ll} & g_{lr} \end{bmatrix}$$

where $\mathbf{G}_{ul}$ is an $n \times n$ matrix, g_{lr} is the scalar Fisher information for θ_{n+1}, and $\mathbf{g}_{ur} = \mathbf{g}_{ll}^T$ are $n \times 1$ vectors with kth element,

$$\begin{aligned} \mathbf{g}_{ur}(k) &= \mathrm{I}_{H(n+1)}(k)\,\mathrm{E}\left(\tfrac{\partial}{\partial\theta_k} l_{k,n+1}^{n+1}\right)\left(\tfrac{\partial}{\partial\theta_{n+1}} l_{k,n+1}^{n+1}\right), \\ g_{lr} &= \sum_{j\in H(n+1)} \mathrm{E}\left(\tfrac{\partial}{\partial\theta_{n+1}} l_{n+1,j}^{n+1}\right)^2. \end{aligned}$$

Here, we denote the log-likelihood of the observation between devices i and j in (1) as $l_{i,j}^n$ and $l_{i,j}^{n+1}$ for the n and $(n+1)$ blindfolded device cases, respectively. Similarly, let $l^n(\mathbf{X}|\boldsymbol{\gamma}_n)$ and $l^{n+1}(\mathbf{X}|\boldsymbol{\gamma}_{n+1})$ be the joint log-likelihood function in (1) for the n and $n+1$ blindfolded device cases, respectively. Then

$$l^{n+1}(\mathbf{X}|\boldsymbol{\gamma}_{n+1}) = \sum_{i=1}^{m+n+1} \sum_{\substack{j\in H(i) \\ j<i}} l_{i,j}^{n+1} = l^n(\mathbf{X}|\boldsymbol{\gamma}_n) + \sum_{\substack{j\in \\ H(n+1)}} l_{n+1,j}^{n+1}.$$

Since $l_{n+1,j}^{n+1}$ is a function only of parameters $\gamma_{n+1} = \theta_{n+1}$ and γ_j,

$$\frac{\partial^2}{\partial\theta_k\partial\theta_l} \sum_{\substack{j\in \\ H(n+1)}} l_{n+1,j}^{n+1} = \begin{cases} \mathrm{I}_{H(n+1)}(k)\frac{\partial^2}{\partial\theta_k^2} l_{n+1,k}^{n+1}, & l = k \\ 0, & l \neq k \end{cases}$$

Thus $\mathbf{G}_{ul} = \mathbf{F} + \mathrm{diag}(\mathbf{h})$, where $\mathbf{h} = \{h_1, \ldots, h_n\}$ and $h_k = \mathrm{I}_{H(n+1)}(k)\mathrm{E}(\frac{\partial}{\partial\theta_k} l_{n+1,k}^{n+1})^2$. Compare the CRB for the covariance matrix of the first n devices in the n and $n+1$ device cases, given by $\mathbf{F}^{-1}$ and $[\mathbf{G}^{-1}]_{ul}$, respectively. Here, $[\mathbf{G}^{-1}]_{ul}$ is the upper left $n \times n$ submatrix of G^{-1},

$$[\mathbf{G}^{-1}]_{ul} = \left\{\mathbf{G}_{ul} - \mathbf{g}_{ur} g_{lr}^{-1} \mathbf{g}_{ll}\right\}^{-1} = \{\mathbf{F} + \mathbf{J}\}^{-1}$$
$$\text{where} \quad \mathbf{J} = \mathrm{diag}(\mathbf{h}) - \tfrac{\mathbf{g}_{ur}\mathbf{g}_{ur}^T}{g_{lr}}$$

Both $\mathbf{F}$ and $\mathbf{J}$ are Hermitian. We know that $\mathbf{F}$ is positive semidefinite. Let $\lambda_k(\mathbf{F}), k = 1 \ldots n$ be the eigenvalues of $\mathbf{F}$ and $\lambda_k(\mathbf{F}+\mathbf{J}), k = 1 \ldots n$ be the eigenvalues of the sum, both listed in increasing order, then if we can show that $\mathbf{J}$ is positive semidefinite, then it is known [26] that:

$$0 \leq \lambda_k(\mathbf{F}) \leq \lambda_k(\mathbf{F}+\mathbf{J}), \forall k = 1 \ldots n \tag{18}$$

Since the eigenvalues of a matrix inverse are the inverses of the eigenvalues of the matrix,

$$\lambda_k\left(\{\mathbf{F}+\mathbf{J}\}^{-1}\right) \leq \lambda_k(\mathbf{F}^{-1}), \forall k = 1 \ldots n, \tag{19}$$

which proves property 1 of Theorem 1. If in addition, we can show that $\mathrm{tr}(\mathbf{J}) > 0$, then $\mathrm{tr}(\mathbf{F}+\mathbf{J}) > \mathrm{tr}(\mathbf{F})$, and therefore $\sum_{k=1}^{n} \lambda_k(\mathbf{F}+\mathbf{J}) > \sum_{k=1}^{n} \lambda_k(\mathbf{F})$. This with (18) implies that $\lambda_j(\mathbf{F}+\mathbf{J}) > \lambda_j(\mathbf{F})$ for at least one $j \in 1 \ldots n$. Thus in addition to (19),

$$\lambda_j\left(\{\mathbf{F}+\mathbf{J}\}^{-1}\right) < \lambda_j(\mathbf{F}^{-1}), \text{for some } j \in 1 \ldots n$$

which implies that $\mathrm{tr}\left(\{\mathbf{F}+\mathbf{J}\}^{-1}\right) < \mathrm{tr}(\mathbf{F}^{-1})$, which proves property 2 of Theorem 1.

1) Showing positive semidefiniteness and positive trace of $\mathbf{J}$ *:* The diagonal elements of $\mathbf{J}$, $[\mathbf{J}]_{k,k}$ are,

$$[\mathbf{J}]_{k,k} = h_k - \mathbf{g}_{ur}^2(k)/g_{lr}. \tag{20}$$

If $k \notin H(n+1)$ then $h_k = 0$ and $\mathbf{g}_{ur}(k) = 0$, thus $[\mathbf{J}]_{k,k} = 0$. Otherwise, if $k \in H(n+1)$,

$$[\mathbf{J}]_{k,k} = \mathrm{E}\left(\frac{\partial l_{n+1,k}^{n+1}}{\partial \theta_k}\right)^2 - \frac{\left[\mathrm{E}\left(\frac{\partial l_{n+1,k}^{n+1}}{\partial \theta_k}\right)\left(\frac{\partial l_{n+1,k}^{n+1}}{\partial \theta_{n+1}}\right)\right]^2}{\sum_{j\in H(n+1)} \mathrm{E}\left(\frac{\partial l_{n+1,j}^{n+1}}{\partial \theta_{n+1}}\right)^2}.$$

Because of reciprocity, the numerator is equal to the square of the $j = k$ term in the sum in the denominator. Thus

$$[\mathbf{J}]_{k,k} \geq \mathrm{E}\left(\frac{\partial l_{n+1,k}^{n+1}}{\partial \theta_k}\right)^2 - \mathrm{E}\left(\frac{\partial l_{n+1,k}^{n+1}}{\partial \theta_k}\frac{\partial l_{n+1,k}^{n+1}}{\partial \theta_{n+1}}\right) = 0.$$

The equality will hold if k is the only member of the set $H(n+1)$. When condition (2) of Theorem 1 holds, $[\mathbf{J}]_{k,k}$ will be strictly greater than zero. Thus $\mathrm{tr}\mathbf{J} > 0$.

Next, we show that $\mathbf{J}$ is diagonally dominant [26], i.e.,

$$[\mathbf{J}]_{k,k} \geq \sum_{\substack{j=1 \\ j\neq k}}^{n} |[\mathbf{J}]_{k,j}| = \sum_{\substack{j=1 \\ j\neq k}}^{n} \frac{|\mathbf{g}_{ll}(k)\mathbf{g}_{ll}(j)|}{g_{lr}},$$

where $[\mathbf{J}]_{k,k}$ is given in (20). Since $H(n+1) \neq \emptyset$, thus $g_{lr} > 0$, and an equivalent condition is,

$$g_{lr}h_k \geq |\mathbf{g}_{ur}(k)| \sum_{j=1}^{n} |\mathbf{g}_{ur}(j)|. \tag{21}$$

If $k \notin H(n+1)$ then $h_k = 0$ and $\mathbf{g}_{ur}(k) = 0$, and the equality holds. If $k \in H(n+1)$, then

$$g_{lr}h_k = \mathrm{E}\left(\frac{\partial l_{k,n+1}^{n+1}}{\partial \theta_k}\right)^2 \sum_{j\in H(n+1)} \mathrm{E}\left(\frac{\partial l_{n+1,j}^{n+1}}{\partial \theta_{n+1}}\right)^2.$$

Because of condition (1) of Theorem 1,

$$\mathrm{E}\left(\frac{\partial l_{k,n+1}^{n+1}}{\partial \theta_k}\right)^2 = \left|\mathrm{E}\left(\frac{\partial l_{k,n+1}^{n+1}}{\partial \theta_{n+1}}\frac{\partial l_{k,n+1}^{n+1}}{\partial \theta_k}\right)\right|$$

Thus

$$g_{lr}h_k = |\mathbf{g}_{ur}(k)|\left[\sum_{\substack{j\geq 1\\ j\in H(n+1)}}|\mathbf{g}_{ur}(j)| + \sum_{\substack{j\leq 0\\ j\in H(n+1)}}\left|\mathrm{E}\left(\frac{\partial l_{j,n+1}^{n+1}}{\partial \theta_{n+1}}\frac{\partial l_{j,n+1}^{n+1}}{\partial \theta_j}\right)\right|\right]$$

Since $\mathbf{g}_{ur}(j) = 0$ if $j \notin H(n+1)$ we can include in the first sum all $j \in 1 \ldots n$. Since the 2^{nd} sum is ≥ 0, (21) is true.

Diagonal dominance implies $\mathbf{J}$ is positive semidefinite, which proves (19). Note that if $H(n+1)$ includes ≥ 1 reference device, the 2^{nd} sum is > 0 and the inequality in (21) is strictly > 0,which implies positive definiteness of $\mathbf{J}$ and assures that the CRB will strictly decrease.

C. CRB for Location Estimation

For the elements of $\mathbf{F}_R$, using (7) and (1),

$$l_{i,j} = \log\left(\frac{10\log 10}{\sqrt{2\pi\sigma_{dB}^2}}\frac{1}{P_{i,j}}\right) - \frac{b}{8}\left(\log\frac{d_{i,j}^2}{\hat{d}_{i,j}^2}\right)^2.$$

Recall $d_{i,j} = \sqrt{(x_i - x_j)^2 + (y_i - y_j)^2}$. Thus,

$$\frac{\partial}{\partial x_j}l_{i,j} = -b\left(\log\frac{d_{i,j}^2}{\tilde{d}_{i,j}^2}\right)\frac{x_j - x_i}{d_{i,j}^2}.$$

Note that $\frac{\partial}{\partial x_j}l_{i,j} = -\frac{\partial}{\partial x_i}l_{i,j}$, thus the log-normal distribution of RSS measurements meets condition (1) of Theorem 1. The 2^{nd} partials differ based on whether or not $i = j$ and if the partial is taken w.r.t. y_i or x_i. For example,

$$\begin{aligned}\frac{\partial^2 l_{i,j}}{\partial x_j \partial y_j} &= -b\frac{(x_i - x_j)(y_i - y_j)}{d_{i,j}^4}\left[-\log\left(\frac{d_{i,j}^2}{\tilde{d}_{i,j}^2}\right) + 1\right]\\ \frac{\partial^2 l_{i,j}}{\partial x_j \partial y_i} &= -b\frac{(x_i - x_j)(y_i - y_j)}{d_{i,j}^4}\left[\log\left(\frac{d_{i,j}^2}{\tilde{d}_{i,j}^2}\right) - 1\right]\end{aligned}$$

Note that $\mathrm{E}[\log(d_{i,j}^2/\tilde{d}_{i,j}^2)] = 0$. Thus the FIM simplifies to take the form in (10). For the TOA case, the derivation is very similar, and the details are omitted for brevity.

References

[1] Pi-Chun Chen, "A non-line-of-sight error mitigation algorithm in location estimation," in *IEEE Wireless Comm. and Networking Conf.*, Sept. 1999, pp. 316–320.

[2] Maurizio A. Spirito, "On the accuracy of cellular mobile station location estimation," *IEEE Trans. on Veh. Tech.*, vol. 50, no. 3, pp. 674–685, May 2001.

[3] Jeffrey H. Reed, Kevin J. Krizman, Brian D. Woerner, and Theodore S. Rappaport, "An overview of the challenges and progress in meeting the E-911 requirement for location service," *IEEE Comm. Magazine*, pp. 30–37, April 1998.

[4] Jay Werb and Colin Lanzl, "Designing a positioning system for finding things and people indoors," *IEEE Spectrum*, vol. 35, no. 9, pp. 71–78, Sept. 1998.

[5] Andy Ward, Alan Jones, and Andy Hopper, "A new location technique for the active office," *IEEE Personal Comm.*, vol. 4, no. 5, pp. 42–47, Oct. 1997.

[6] Jan M. Rabaey, M. Josie Ammer, Julio L. da Silva, Jr., Danny Patel, and Shad Roundy, "Picorodio supports ad hoc ultra-low power wireless networking," *IEEE Computer*, vol. 33, no. 7, pp. 42–48, July 2000.

[7] Robert Fleming and Cherie Kushner, "Low-power, miniature, distributed position location and communication devices using ultra-wideband, nonsinusoidal communication technology," Aetherwire Inc., Semi-Annual Technical Report, ARPA Contract J-FBI-94-058, Tech. Rep., July 1995.

[8] Randolph L. Moses, Dushyanth Krishnamurthy, and Robert Patterson, "An auto-calibration method for unattended ground sensors," in *ICASSP*, vol. 3, May 2002, pp. 2941–2944.

[9] Dennis D. McCrady, Lawrence Doyle, Howard Forstrom, Timothy Dempsy, and Marc Martorana, "Mobile ranging with low accuracy clocks," *IEEE Trans. on Microwave Theory and Techniques*, vol. 48, no. 6, pp. 951–957, June 2000.

[10] Andreas Savvides, Heemin Park, and Mani B. Srivastava, "The bits and flops of the n-hop multilateration primitive for node localization problems," in *Intl. Workshop on Sensor Nets. & Apps.*, Sept. 2002, pp. 112–121.

[11] Srdan Čapkun, Maher Hamdi, and Jean-Pierre Hubaux, "GPS-free positioning in mobile ad-hoc networks," in 34^{th} *IEEE Hawaii Int. Conf. on System Sciences (HICSS-34)*, Jan. 2001.

[12] Joe Albowicz, Alvin Chen, and Lixia Zhang, "Recursive position estimation in sensor networks," in *IEEE Int. Conf. on Network Protocols*, Nov. 2001, pp. 35–41.

[13] Chris Savarese, Jan M. Rabaey, and Jan Beutel, "Locationing in distributed ad-hoc wireless sensor networks," in *ICASSP*, May 2001, pp. 2037–2040.

[14] Radhika Nagpal, Howard Shrobe, and Jonathan Bachrach, "Organizing a global coordinate system from local information on an ad hoc sensor network," in *2nd Intl. Workshop on Inform. Proc. in Sensor Networks*, April 2003.

[15] Lance Doherty, Kristofer S. J. pister, and Laurent El Ghaoui, "Convex position estimation in wireless sensor networks," in *IEEE INFOCOM*, vol. 3, 2001, pp. 1655 –1663.

[16] Neal Patwari, Robert J. O'Dea, and Yanwei Wang, "Relative location in wireless networks," in *IEEE VTC*, vol. 2, May 2001, pp. 1149–1153.

[17] Kaveh Pahlavan, Prashant Krishnamurthy, and Jacques Beneat, "Wideband radio propagation modeling for indoor geolocation applications," *IEEE Comm. Magazine*, pp. 60–65, April 1998.

[18] Homayoun Hashemi, "The indoor radio propagation channel," *Proceedings of the IEEE*, vol. 81, no. 7, pp. 943–968, July 1993.

[19] Alfred O. Hero III. Electronic version of this article. [Online]. Available: http://www.eecs.umich.edu/~hero/comm.html

[20] Neal Patwari, Yanwei Wang, and Robert J. O'Dea, "The importance of the multipoint-to-multipoint indoor radio channel in ad hoc networks," in *IEEE Wireless Comm. and Networking Conf.*, March 2002, pp. 608–612.

[21] Theodore S. Rappaport, *Wireless Communications: Principles and Practice*. New Jersey: Prentice-Hall Inc., 1996.

[22] Alfred O. Hero III, Jeffrey A. Fessler, and Mohammad Usman, "Exploring estimator bias-variance tradeoffs using the uniform CR bound," *IEEE Trans. on Sig. Proc.*, vol. 44, no. 8, pp. 2026–2041, Aug. 1996.

[23] Benjamin B. Peterson, Chris Kmiecik, Richard Hartnett, Patrick M. Thompson, Jose Mendoza, and Hung Nguyen, "Spread spectrum indoor geolocation," *Journal of the Institute of Navigation*, vol. 45, no. 2, pp. 97–102, Summer 1998.

[24] Alan J. Coulson, Allan G. Williamson, and Rodney G. Vaughan, "A statistical basis for lognormal shadowing effects in multipath fading channels," *IEEE Trans. on Veh. Tech.*, vol. 46, no. 4, pp. 494–502, April 1998.

[25] Greg Durgin, Theodore S. Rappaport, and Hao Xu, "Measurements and models for radio path loss and penetration loss in and around homes and trees at 5.85 GHz," *IEEE Journal on Sel. Areas in Comm.*, vol. 46, no. 11, pp. 1484–1496, Nov. 1998.

[26] Roger A. Horn and Charles R. Johnson, *Matrix Analysis*. New York: Cambridge Univ. Press, 1990.